Journal of
Materials Chemistry C

Materials for optical, magnetic and electronic devices

Accepted Manuscript

This article can be cited before page numbers have been issued, to do this please use: T. Chowdhury, R. Khatun, R. Rahaman and Md. A. Rahman, *J. Mater. Chem. C*, 2025, DOI: 10.1039/D5TC02386F.

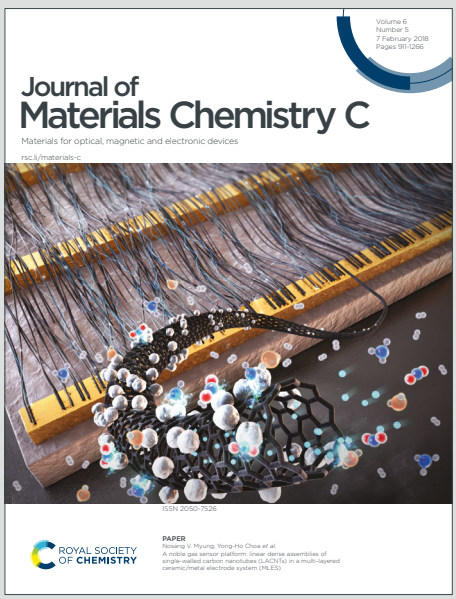

ROYAL SOCIETY OF CHEMISTRY

rsc.li/materials-c

View Article Online
DOI: 10.1039/D5TC02386F

Cadmium defect-induced modulation of hole self-trapping in monoclinic gallium oxide for optoelectronic applications

Tasfia Chowdhury, Rahima Khatun, Md. Rabiur Rahaman, and M. Azizar Rahman*

Department of Physics, Bangladesh University of Engineering and Technology, Dhaka-1000, Bangladesh

* Corresponding author. Email: azizar@phy.buet.ac.bd

ABSTRACT

Self-trap holes (STHs) in β-Ga_2O_3 prohibit p-type conduction in this material, severely limiting the homojunction-based optoelectronic applications. Here, we report that the presence of cadmium (Cd) impurity in β-Ga_2O_3 ($CdGa_2O_3$) drastically quenches STHs and significantly increases p-type conductivity in this material, making it promising for optoelectronics. Photoluminescence experiments show that Cd-induced defects in β-Ga_2O_3 significantly suppress the characteristic ultraviolet luminescence, indicating the reduction of STHs. The $CdGa_2O_3$ film shows the distinct recombination channels of green and blue emissions attributed to Cd_{Ga} and V_{Ga} defects, which exhibit slow decay time constants of 38.45 and 13.31μs, respectively. Density functional calculations reveal that a few atom% of Cd in β-Ga_2O_3 induces an intermediate valence band state due to the formation of Cd_{Ga} and V_{Ga} defects in the octahedral sites. The calculated energy levels of Cd_{Ga} and V_{Ga} defects are 0.72 and 0.18 eV, respectively, which are significantly lower than the energy levels of 0.99 eV for STHs, resulting in the destabilization of STHs and promoting p-type conductivity. The Mott-Schottky measurement confirms the p-type conductivity in $CdGa_2O_3$ film with an acceptor concentration of 3.65×10^{17} cm^{-3}. This p-type $CdGa_2O_3$ film is used in fabricating Ag/p-$CdGa_2O_3$ Schottky diodes, which operate as high-performance self-powered ultraviolet photodetectors possessing a high responsivity of 164 mA/W and specific detectivity of 7.5×10^{11}Jones. This p-type

$CdGa_2O_3$ film could provide better flexibility in designing efficient homojunction-based optoelectronic devices.

Keywords: p-type $CdGa_2O_3$, Cd-induced defects, Self-trap holes, Schottky diodes, Photodetectors,

1. Introduction

Gallium oxide (Ga_2O_3) crystallizes in various phases such as α, β, γ, δ, and ε.[1] Among all phases, monoclinic β-Ga_2O_3 is the most stable phase, and it has an ultra-wide optical bandgap of 4.8 eV and a high breakdown electric field of 13 MV cm^{-1}, which are promising for power electronics.[2, 3] However, these applications are restricted owing to the poor understanding of acceptor impurities and the lack of a highly conductive p-type β-Ga_2O_3 layer. β-Ga_2O_3 is an inherently n-type semiconducting material, but recently, Chikoidze et al. reported p-type conductivity in this material.[4] Moreover, oxygen vacancy has a lower formation energy in β-Ga_2O_3 and is present in a significant concentration, compensating for the acceptor density.[5] Moreover, the self-trapped holes are easily formed in β-Ga_2O_3 and act as polaronic acceptors, prohibiting p-type conductivity.[6] First-principle calculations have shown that Cd, Cu, N, and Zn are promising acceptor impurities for achieving p-type β-Ga_2O_3.[7] Experimental studies reported that N- and Zn-doped β-Ga_2O_3 have shown a low free hole density in the range of 10^{14}-10^{15} cm^{-3}, which is insufficient to fabricate efficient power electronic devices.[8, 9] Density functional calculations have shown that Cd preferably occupies the Ga site (Cd_{Ga}), acting as an acceptor in β-Ga_2O_3, and this defect is effective in modifying the near valence-band structure and optoelectrical properties of this material,[10] however, experimental studies of the Cd-induced defects on the optoelectrical properties of β-Ga_2O_3 have not been conducted.

Monoclinic β-Ga_2O_3 typically shows blue emission in the 2.8-3.0 eV energy range and ultraviolet emission in the 3.3-3.4 eV energy range.[11] The ultraviolet emissions are attributed to the self-trap hole, while the blue emission is attributed to gallium vacancy (V_{Ga}).[11] The

View Article Online
DOI: 10.1039/D5TC02386F

presence of a significant amount of V_{Ga} in β-Ga_2O_3 contributes to p-type conductivity in this material.[12] Moreover, the optical bandgap and electrical properties of β-Ga_2O_3 can be modulated significantly by alloying with CdO.[13, 14] However, the effect of Cd-induced defects on the luminescence properties of β-Ga_2O_3 and their recombination kinetics has not yet been studied.

This research focuses on the combined experimental and theoretical analysis of the influence of Cd-induced defects on the optical, electronic, and electrical properties of β-Ga_2O_3 thin films and utilizes this material in power electronic and photodetector devices. The current work also examines the simulation of steady-state and transient luminescence spectral line shapes to determine the energy position of Cd dopants-induced defects, the zero-phonon line energy, electron-phonon coupling strength, and carrier dynamics in β-Ga_2O_3 films.

2. Experimental Section

2.1 Material and Synthesis

Pristine and $CdGa_2O_3$ films were synthesized on glass substrates and indium tin oxide (ITO)-coated glass using an atomizing spray pyrolysis technique. Highly pure (99.9% Sigma Aldrich) $Ga(NO_3)_3$. xH_2O and $Cd(CH_3COO)_2 \cdot 2H_2O$ were mixed in the deionized water to obtain a solution of 0.05 M, containing Cd concentrations of up to 15 atom%. The film thickness (200 ± 20) nm was kept constant by adjusting the deposition time and the spray rate. The structure, morphology, and chemical analysis of the films were investigated using an X-ray diffractometer (XRD), scanning electron microscope (SEM), an energy-dispersive X-ray spectrometer (EDS), and X-ray photoelectron spectra (XPS). Optical properties of the films were studied by UV-VIS and FS5 photoluminescence spectrometers. The carrier type and concentration were measured using an electrochemical workstation.

View Article Online
DOI: 10.1039/D5TC02386F

2.2 Device Fabrication

For the fabrication of Ag/$CdGa_2O_3$ Schottky diodes, a 200 nm thick layer of $CdGa_2O_3$ was deposited on a glass substrate using a shadow mask of 5x5 mm^2. The silver was used as an electrode material for the Schottky contact on $CdGa_2O_3$ films. A thin layer of Ag was deposited on $CdGa_2O_3$ films to fabricate the Ag/$CdGa_2O_3$ Schottky diodes. The current-voltage (*I-V*) characteristics of power devices were analyzed using a Keithley source measuring unit. The photodetection properties of the Ag/$CdGa_2O_3$ Schottky photodiodes were measured using a UV light source of wavelength 365 nm and power 500μW/cm^2.

2.3 Theoretical details

First-principles calculations were performed to investigate the Cd-induced defects in β-Ga_2O_3. A 1 x 1 x 2 supercell of β-Ga_2O_3, consisting of 16 gallium and 24 oxygen atoms, was investigated. The Cd_{Ga} and V_{Ga} defects structure was introduced by substituting or removing a Cd atom in the same structure. The substitution of two Cd atoms leads to a defect density of (2/16) ~12 atom%. The DFT + U method was applied for this investigation, with a U_d value of 7 eV for Cd-4d orbitals and the U_p value of 7 eV for O-2p orbitals.[15] A Hubbard U value of 7 was considered to align the theoretical bandgap with the experimental data, addressing the underestimation issue of the standard GGA-PBE methods. All computations were done in this investigation, applying the CASTEP.[16] The energy positions of luminescence centers are estimated using the configuration coordinate model and Franck-Condon approximation.[17] The luminescence centers in wide bandgap materials typically act as electron-phonon (e-p) coupling. This e-p coupling strength redshifts the defect luminescence band corresponding to the localized states. The e-p coupling strength (S) for wide band gap semiconducting material is high. For the semiconducting materials with high e-p coupling (S >>1), the spectral line

View Article Online
DOI: 10.1039/D5TC02386F

shape of the steady-state photoluminescence (I_{PL}) can be calculated by the following equation.[18]

$$I_{PL}(\hbar\omega) \sim \sum_n exp(-S)\frac{S^n}{n!} \times exp\left[\frac{1}{2\sigma} \times (E_{ZPL} - n\hbar\omega_{LO} - \hbar\omega)^2\right] \quad (1)$$

where, $\hbar\omega$ is the photon energy, n is the number of phonons, and ω_{LO} longitudinal optics phonon frequency. The key parameters in expression (1) that generate the PL spectral line shape are: (i) σ stand for the emission bandwidth ($FWHM = \sqrt{8ln2}\,\sigma$), (ii) S is the Huang-Rhys factor, which calculates the PL peak energy, and (iii) E_{ZPL} estimates the energy position of defects in the bandgap.

3. Results and Discussion

3.1 Structural, Morphological, and Electronic Properties

Figure (a)-(b) shows the SEM images of Ga_2O_3 and $CdGa_2O_3$ films. Both films show smooth surfaces containing a uniform distribution of spherical grains. The grain size of pristine Ga_2O_3 is in the range of 15-30 nm, and slightly increases for $CdGa_2O_3$ film, resulting from the higher atomic size of Cd^{2+} (95 pm) than that of Ga^{3+} (62 pm). The Cd concentration in $CdGa_2O_3$ is confirmed by an EDS spectrometer and found to be 9.95 (~10) atom% [Figure S1 and Table S1]. XRD patterns of pristine and $CdGa_2O_3$ films with various Cd concentrations are displayed in Figure 1(c). XRD patterns confirm the formation of a monoclinic structure for both the pristine and $CdGa_2O_3$ films. At higher doping levels of Cd (>10 atom%), the film becomes an alloy structure of CdO-Ga_2O_3. The β-Ga_2O_3 film with 10 atom% Cd was selected for this investigation to limit this study to a pure monoclinic structure of β-Ga_2O_3. The monoclinic structure of $CdGa_2O_3$ film remains unchanged when the film is annealed at 900 ºC under a vacuum environment [Figure S2]. All XRD orientations are explored from the JCPDS card no. 75-0592 for β-Ga_2O_3 and identified as (110) crystallographic orientation for the pristine β-Ga_2O_3 and (002), (110) orientations for $CdGa_2O_3$ films. The observed (111), (200), and (220)

crystallographic orientations in the film with the high doping level of Cd are for cubic CdO. The Cd in β-Ga_2O_3 causes significant modification of the structural properties of the β-Ga_2O_3 film. The (111) crystallographic orientation of the pristine β-Ga_2O_3 film shifts to lower Bragg angles in the $CdGa_2O_3$ film. This shifting of the XRD peak position is due to the incorporation of Cd^{2+}, which has a larger ionic radius (0.092 nm) than that of Ga^{3+}(0.062 nm).

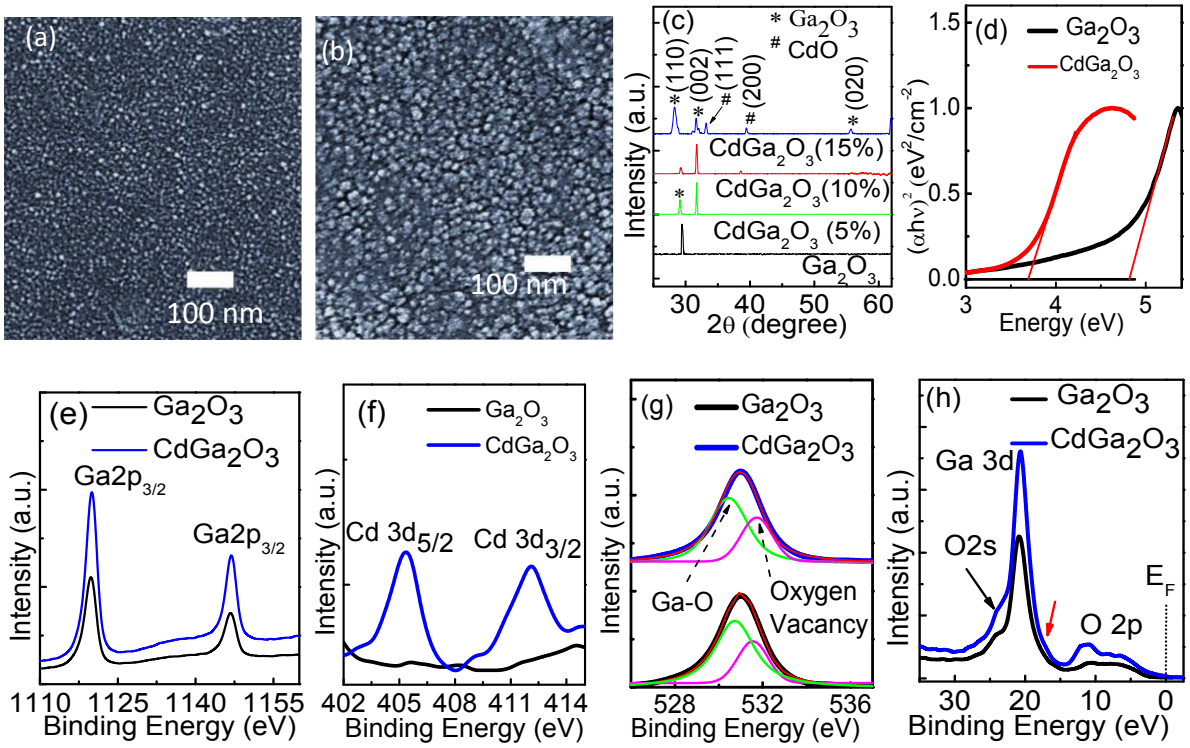

Figure 1. (a) and (b) show SEM images of Ga_2O_3 and $CdGa_2O_3$ films. The films show spherical grains uniformly distributed throughout the film. (c) The XRD pattern of pristine and $CdGa_2O_3$ thin films confirms the formation of a monoclinic structure in both films. (d) Tauc's plot for the determination of the optical band gap of Ga_2O_3 and $CdGa_2O_3$ films. The pristine films show a band gap of 4.8 eV, which is reduced to 3.68 eV for the $CdGa_2O_3$ film. (e) Ga 2p doublets are separated by a binding energy difference of 27 eV. (f) Cd 3d doublets are separated by an energy interval of 6.7 eV. The peak nature and energy position of the Ga 2p peak demonstrate that the valence state of Ga is Ga^{3+}, without any intermediate valence states. (g)The O 1s peak of pristine and $CdGa_2O_3$ films and the deconvolution of the O 1s peak gives two components

View Article Online
DOI: 10.1039/D5TC02386F

at 530.48 eV and 531.68 eV. (h) Near valence band XPS spectra of pristine and $CdGa_2O_3$ thin films. The valence band maxima for Ga_2O_3 and $CdGa_2O_3$ films are 2.4 and 1.6 eV, respectively [Figure S2].

The optical bandgap of β-Ga_2O_3 films has been estimated from Tauc's plot [Figure 1 (d)] and found to be 4.8 eV, which decreased to 3.68 eV for the $CdGa_2O_3$ film. This decrease in the optical bandgap is associated with Cd-induced defects, where the Cd occupying a Ga site (Cd_{Ga}) acts as an acceptor in the film. The formation of Cd_{Ga} acceptors forms a defect state above the valence band. At a high level of Cd, the wavefunctions of Cd_{Ga} acceptors induce an impurity band that subsequently merges with the valence band, decreasing the band gap.

Figure 1(e) displays the core-level photoelectron spectra of the Ga 2p doublet for both Ga_2O_3 and $CdGa_2O_3$ films. The binding energy values of the Ga $2p_{3/2}$ and Ga $2p_{1/2}$ peaks are found to be at 1120.0 and 1145.0 eV, respectively, and show no significant change with the incorporation of Cd dopant. The analysis of the Ga 2p peak provided insights into the Ga valence state. The energy position and nature of the Ga 2p peak indicate that Ga exists in its highest valence state, Ga^{3+}, without any intermediate valence states. The peak-to-peak difference between the Ga 2p doublet is 27 eV, consistent with the previously reported data for Ga 2p.[19] Figure 1 (f) shows the Cd 3d core-level spectra of the $CdGa_2O_3$ film. The Cd $3d_{5/2}$ and Cd $3d_{3/2}$ doublet peaks are observed at 405.48 and 412.18 eV binding energy, respectively. The double is separated by 6.7 eV. This result indicates the presence of Cd^{2+} state in $CdGa_2O_3$ films.[20] The X-ray photoelectron spectra of the high-resolution O 1s of the pristine and $CdGa_2O_3$ films are shown in Figure 1 (g). The Gaussian function was employed to deconvolute the O 1s core level, which shows two peaks at 530.48 and 531.68 eV. The 530.48 eV peak is related to lattice oxygen (Ga-O), while the peak at 531.68 eV is associated with oxygen vacancies (V_o).[19] The high binding energy peak at 531.5 eV of the O 1s spectra is almost

View Article Online
DOI: 10.1039/D5TC02386F

identical for pristine and $CdGa_2O_3$ films, indicating the oxygen vacancy concentration remains unchanged in both films. The Oxygen vacancy level has not significantly changed in the Cd-doped Ga_2O_3 film. In Cd-doped Ga_2O_3 film, the Cd_{Ga} and V_{Ga} acceptor concentrations increase. The oxygen vacancy gets a chance to recombine with Cd_{Ga} and V_{Ga} acceptors, resulting in the intense blue and green emissions. The oxygen vacancy concentration has not significantly changed because the formation of more Cd_{Ga} and V_{Ga} acceptors creates an opportunity for oxygen vacancies to recombine with these acceptor defects. While oxygen vacancies induce n-type conductivity, Cd_{Ga} and V_{Ga} acceptor dopants can compensate for these defects and potentially lead to p-type conductivity. The potential limit of compensation depends on the energy levels at which the acceptor dopants introduce holes, affecting their potential to compensate for electrons from oxygen vacancies. From the photoluminescence analysis, it is observed that the Cd_{Ga} is a deep-type acceptor, while the V_{Ga} is a shallow-type acceptor in Cd-doped Ga_2O_3 films. The potential compensation of the oxygen vacancy is caused by the V_{Ga} and Cd_{Ga} defecta. The near valence band XPS spectra of pristine and $CdGa_2O_3$ films are displayed in Figure 1 (h). Three distinct core levels of O 2s, O 2p, and Ga 3d are observed in the near valence band spectra of both the pristine and $CdGa_2O_3$ films. The broad peak at 20.8 is due to the superposition of O 2s at 24.0 eV and Ga 3d at 20.8 eV. A small shoulder is found at 19.0 eV (indicated by the red arrow symbol), which is attributed to the hybridization of O 2s and Ga 3d.[21] The broad O 2p core-level peak with a full-width half maxima (FWHM) of 7.9 eV owing to the contribution of the three oxygen sites of β-Ga_2O_3.[21] The valence band maxima of pristine and $CdGa_2O_3$ films have been determined from the linear extrapolation method and found to be 2.4 and 1.6 eV for the pristine and $CdGa_2O_3$ films, respectively [Figure S3 (a) and (b)].

View Article Online
DOI: 10.1039/D5TC02386F

3.2 Cadmium-Induced Defect Luminescence

Figure 2(a) shows photoluminescence (PL) spectra (open circles) of pristine and $CdGa_2O_3$ films at room temperature. The PL bands in the pristine and $CdGa_2O_3$ films are broad, resulting from strong electron-phonon coupling.[22] The deconvolution of PL spectra is required to understand the luminescence properties of these films. The PL spectra were deconvoluted using the Gaussian fitting methods as previously described in β-Ga_2O_3 films.[23] The Gaussian fitting spectra (solid lines) for pristine and $CdGa_2O_3$ films are also shown in Figure 2 (a). Using this method, the PL spectra of the pristine β-Ga_2O_3 films are deconvoluted with two emission bands peaking at 3.30 ± 0.02 and 2.98 ± 0.02 eV with a corresponding full width at half maximum of 0.55 ± 0.03 and 0.58 ± 0.03 eV, respectively. The 2.98 and 3.30 eV emission bands have been assigned as blue luminescence (BL) and ultraviolet luminescence (UVL), respectively. For $CdGa_2O_3$ films, the PL spectrum is deconvoluted with an intense BL band with the same FWHM and peak position of the pristine β-Ga_2O_3 film and a green luminescence (GL) band at 2.38 eV with an FWHM of 0.56 ± 0.05. As the BL band is observed in both pristine and $CdGa_2O_3$ films, the peak parameter of the BL band was kept constant for pristine and $CdGa_2O_3$ films to avoid uncertainty in fitting. These BL and UVL bands are the intrinsic property of pristine β-Ga_2O_3 films and are attributed to gallium vacancy (V_{Ga}) and STHs, respectively.[11] The broadening of PL spectral lineshape and significant quenching of the UVL band are observed in $CdGa_2O_3$ film, resulting in the reduction of STHs and introducing a new recombination channel of GL along with the intrinsic BL bands of the pristine film. This result indicates that the Cd-induced defects play a crucial role in rebating the STHs and generating GL bands in $CdGa_2O_3$ film. We proposed that this GL band in the $CdGa_2O_3$ film is attributed to the recombination of the Cd_{Ga} acceptor with a conduction band electron or oxygen vacancy defects in this material. The presence of strong BL and GL in $CdGa_2O_3$ films indicates a high concentration of Cd_{Ga} and V_{Ga} acceptor defects in this film. To obtain further information on

View Article Online
DOI: 10.1039/D5TC02386F

these defects in $CdGa_2O_3$ films, the steady-state PL spectral line shape of BL and GL was simulated within the framework of the configuration coordinate model. [18]

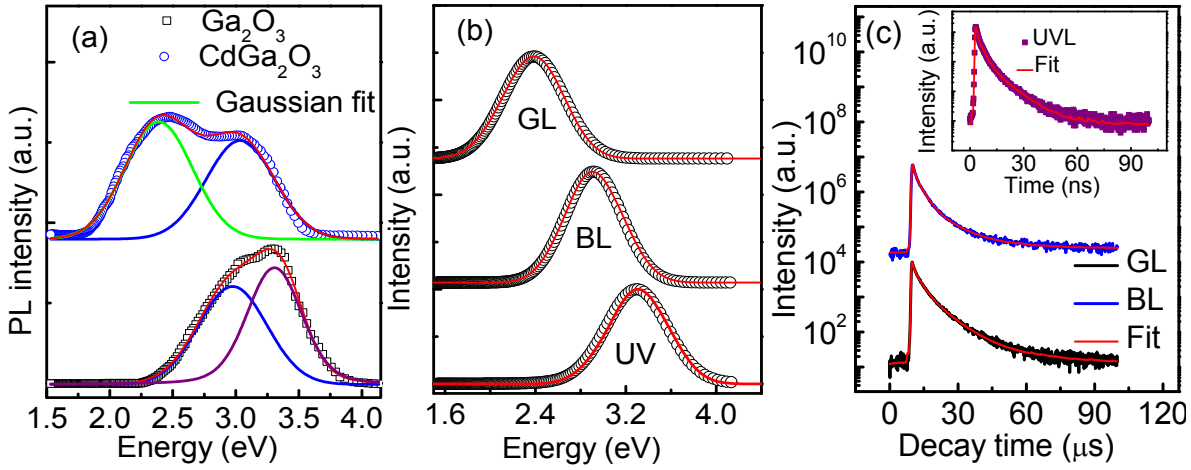

Figure 2. (a) Photoluminescence spectra (open circles) of pristine and $CdGa_2O_3$ thin films at room temperature, and the deconvoluted PL spectra (solid lines) using the Gaussian peak fitting method. Ultraviolet and blue emission bands are observed at 3.30 and 2.98 eV for pristine and $CdGa_2O_3$ film showing the green and blue emission bands at 2.38 and 2.98 eV, respectively. (b) Theoretically obtained PL spectra (solid red lines) for ultraviolet, blue, and green emission bands using the configuration coordinate model are consistent with the experimentally observed PL (open circles). (c) Transient PL decay curves were measured for the 2.38 eV green and 3.0 eV blue bands. The inset of (c) displays the transient PL spectrum for the ultraviolet emission band measured at the central wavelength of 3.30 eV.

The energy position of the blue luminescence center, $V_{Ga,}$ and the green luminescence centers, Cd_{Ga}, have been determined using the configuration coordinate model.[18] The PL spectral line shape of the blue and green emission bands has been calculated theoretically using the configuration coordinate equation (1) and is displayed in Figure 2(b), indicated by the solid line. The experimental photoluminescence spectra are also shown in Figure 2(b) and are indicated by an open circle. The theoretical PL spectra agree with the experimental spectra for

the following parameters: $\omega_{LO} = 71$ meV, $E_{ZPL} = 3.9$ eV, $\sigma = 0.15\,eV$ eV, and S = 8.5 for the UVL band; $\hbar\omega_{LO} = 71$ meV, $E_{ZPL} = 3.5$ eV, $\sigma = 0.15\,eV$ eV, and S = 8.5 for the BL band and $\hbar\omega_{LO} = 71$ meV, $E_{ZPL} = 2.96$ eV, $\sigma = 0.18\,eV$ eV, and S = 8.3 for the GL band. The energy position of the V_{Ga} and Cd_{Ga} luminescence centers involved in the recombination mechanism of blue and green emission bands can be estimated using the following equation as: $E_A = E_g - E_{ZPL}$, where E_A is the acceptor state involved in this recombination channel, and E_g is the optical bandgap of the corresponding material.[24] The Huang-Rhys factors for the BL and GL agree with the literature value of pristine β-Ga_2O_3 films.[25, 26] The high value of *S* in $CdGa_2O_3$ film indicates strong electron-phonon coupling at the deep centers, leading to the significant broadening of the BL emission band. Considering 3.68 eV, the optical band gap of $CdGa_2O_3$ film at room temperature, the energy levels of the blue luminescence centers V_{Ga} and green luminescence centers Cd_{Ga} are estimated and found to be 0.18 and 0.72 eV, respectively, above the valence band maximum. These defects act as acceptor defects in $CdGa_2O_3$ films. The energy position of STHs in $CdGa_2O_3$ is found to be 0.9 eV.

The recombination dynamics of UVL, BL, and GL have been investigated by time-resolved PL (TRPL). Figure 2 (c) displays the room temperature TRPL spectra measured at central wavelengths of 376 nm (UVL), 416 nm (BL), and 521 nm (GL) to investigate the decay time of UVL, BL, and GL color centers. The TRPL spectra are best fitted with triexponential decay time and can be expressed as: $I(t) = B_1\exp(t/\tau_1) + B_2\exp(t/\tau_2) + B_1\exp(t/\tau_3)$, where *I* indicates the TRPL intensity, $B_{1,2,3}$ are the constant and $\tau_{1,2,3}$ are the decay life times.[27] The mean decay time constants have been calculated using the equation; $\langle\tau\rangle = \sum_i A_i\tau_i^2 / \sum_i A_i\tau_i$.[27] The transient PL is well-fitted with triexponential decay constants as: $\tau_1 = 2.55\,\mu s$, $\tau_2 = 8.75\,\mu s$, and $\tau_3 = 64.68\,\mu s$, $\langle\tau\rangle = 38.45\,\mu s$ for BL; $\tau_1 = 4.65\,\mu s$, $\tau_2 = 18.52\,\mu s$, and $\langle\tau\rangle = 13.31\,\mu s$ for GL and $\tau_1 = 0.60\,ns$, $\tau_2 = 2.90\,ns$, $\tau_3 = 10.60\,ns$, and $\langle\tau\rangle = 4.5$ ns for UVL. The fast decay time constant for UVL emission is found to be 4.5 *ns*, consistent with the previous

View Article Online
DOI: 10.1039/D5TC02386F

report.[28] The GL component $CdGa_2O_3$ films show a faster decay time constant of 13.31 μs than the BL component of 38.45 μs, suggesting a different recombination channel involved in the GL band. Incorporating Cd into β-Ga_2O_3 boosts the transfer of energy to the luminescence centers responsible for the green emission band, leading to the fast decay time constant of the GL centers and a much more intense visible luminescence compared to the BL band. The slower decay lifetimes for BL and GL bands reveal that these luminescence bands are attributed to the recombination of a conduction band electron and defect levels formed above the valence band.

3.3 Electrical Properties of $CdGa_2O_3$-Based Heterojunction

The electrochemical impedance spectroscopic technique is employed to identify the carrier type and estimate the carrier concentration of the pristine and $CdGa_2O_3$ films from the Mott-Schottky measurement. Before the Mott-Schottky analysis, cyclic voltammetry (C-V) measurement was performed to identify the suitable voltage range for the electrochemical reactions. Figure 4 (a) and (b) show C-V plots for Ga_2O_3 and $CdGa_2O_3$ films. The C-V analysis indicates that the curves remain undistorted within the -0.5 to 1.0 voltage range for pristine and -1.3 to -0.9 voltage range for $CdGa_2O_3$ films, which is considered the working window for the Mott-Schottky analysis. The Mott-Schottky expression can be expressed as:[29]

$$\frac{1}{C_{sc}^2} = \frac{2}{\varepsilon\varepsilon_o e A^2 N_a}\left(V - V_{fb} - \frac{kT}{e}\right) \quad \text{.....(2)}$$

where, C stands for the capacitance of the space charge layer, A indicates the active area of the film, N_a stands for the acceptor density, V_{fb} is the flat band potential, V is the applied potential, T is the temperature, and k is the Boltzmann constant. The ε and ε_o are the relative permittivity and the free space permittivity of β-Ga_2O_3, respectively. The relative permittivity for β-Ga_2O_3 is 12.4 used for this calculation.[30]

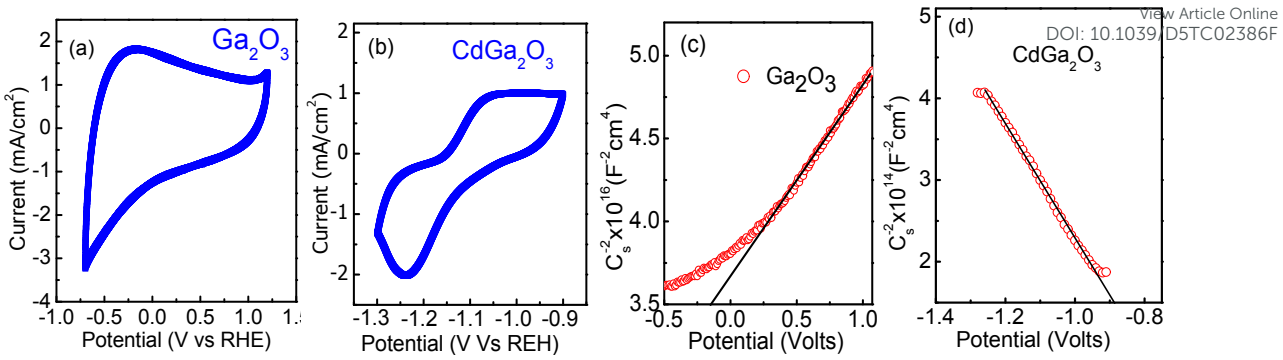

Figure 3. Cyclic voltammetry plots for (a) Ga_2O_3 and (b) $CdGa_2O_3$ films. These narrow voltage windows were considered because the films show more stability under the reaction mechanism at this potential range. Mott-Schottky plot for (c) Ga_2O_3 and (d) $CdGa_2O_3$ films.

Figures 3 (c) and (d) show the Mott-Schottky plot of the Ga_2O_3 and $CdGa_2O_3$ thin films. The positive slopes of pristine β-Ga_2O_3 films indicate that this film has an n-type semiconductor nature. The negative slopes of $CdGa_2O_3$ reveal that this film represents p-type conductivity. The electron density in the pristine and hole density in $CdGa_2O_3$ can be achieved from the slope of the Mott-Schottky plot, where $N_{a(n)} = \frac{2}{\varepsilon\varepsilon_o e A^2}(slope)$. The electron density is 7.4 x 10^{14} cm^{-3} for the pristine β-Ga_2O_3 film. The hole density is 3.65 x10^{17} cm^{-3} for $CdGa_2O_3$ films. The flat band potential (V_{fb}) was determined from the intercept on the voltage axis of the Mott-Schottky plot. The calculated value of V_{fb} is 0.88 eV. The resistance and mobility of $CdGa_2O_3$ film were determined from the Nyquist plot [Figure S4]. The conductivity (σ) can be estimated using the following equation: $\sigma = \frac{1}{R_p} \times \frac{t}{A}$, where, R_p is the parallel resistance modelled with the constant phase element (CPE), t is the film thickness (200 nm) and A ($2.3 \times 10^{-7}\ m^2$) is the cross sectional area of the deposited electrode. Employing the Zview software, the Nyquist plot was fitted according to the provided circuit diagram (inset of Figure S4), and the values for the R_p for $CdGa_2O_3$ film is 10500 ohms. The carrier mobility (μ) is associated to σ by the following equation: $\sigma = N_A q \mu$, where N_A is the acceptor density, q is the magnitude of charge

and μ is the hole mobility. Using the hole density estimated from Mott-Schottky plot, the value of the hole mobility for $CdGa_2O_3$ film is found to be 14.13 cm^2/ Vs. The p-type conductivity is also examined by fabricating the Ga_2O_3 film-based homojunction devices. A 200 nm layer of vanadium (V)-doped Ga_2O_3 (VGa_2O_3) film on an ITO-coated glass substrate, followed by the deposition of $CdGa_2O_3$ film on the V-doped Ga_2O_3 film. The forward current-voltage characteristic of n-type VGa_2O_3/p-type $CdGa_2O_3$ homojunction diodes [Figure S5], which exhibits the rectifying characteristics of the semiconducting diode.

3.4 Performance of $CdGa_2O_3$ as a Self-powered Photodetector.

The p-type $CdGa_2O_3$ films with an optical bandgap of 3.68 are sensitive to ultraviolet light. The inset of Figure 4(a) shows the schematic diagram of Ag/$CdGa_2O_3$ Schottky photodiodes. Figure 4 (a) shows the current-voltage characteristics of a typical Ag/$CdGa_2O_3$ Schottky photodiode under dark and illumination. The current-voltage curve of the Ag/$CdGa_2O_3$ Schottky diode shows a typical rectifying behavior, stipulating the development of the Schottky barrier at the interface of the Ag/$CdGa_2O_3$ junction. The device current increases significantly under illumination of 365 nm, indicating that the fabricated Schottky diodes are sensitive to ultraviolet light. The UV photoelectric properties of Ag/$CdGa_2O_3$ Schottky photodiode are investigated by ultraviolet light of wavelength 365 nm with an optical power of 500 μW/cm^2. Figure 4 (b) shows the time-dependent photo response behavior by periodically switching on and off the source with an optical power of 500 μW/cm2 under an external applied voltage of 0 volts. The dark current is found to be approximately 0.88 μA. When the UV light source was switched on, the photocurrent instantaneously increased to 10.74 μA under zero bias voltage. The current intensity ratio of I_{photo}/I_{dark} is roughly 10 times the value of the dark current. The photocurrent is decreased to the initial dark current when the light source is switched off. The result indicates that the Ag/$CdGa_2O_3$ Schottky photodetector operates without any bias voltage, indicating the self-powered characteristics of photodiodes.

View Article Online
DOI: 10.1039/D5TC02386F

The sensitivity of the photodetector has been calculated by measuring the responsivity (R) and the value of R can be expressed by the following equation:[31] $R = (I_{photo} - I_{dark})/PS$, I_{photo} is the current under illumination, I_{dark} stands for the current under dark condition, P indicates the intensity of the UV light source, and S is the operative illuminated zone of the detector. [32] Under 365 nm illumination, the responsivity was found to be 164 mA/W obtained for the Ag/Ga_2O_3 photodetector. This increased photoresponsivity resulted from enhanced light absorption efficiency and increased collection of electron-hole pairs within the device. A significant concentration of oxygen vacancies is present in the sample, and Cd doping increases the hole concentrations, resulting in an increase in electron-hole pairs in the sample. The figure of merit of a photodetector is investigated by measuring the detectivity (D), and can be described by the following expression: $D = R/(2eJ)^{0.5}$, where J is the current density under dark condition. The value of D is found to be 7.5×10^{11} Jones under zero bias and 500 μW/cm^2 power.

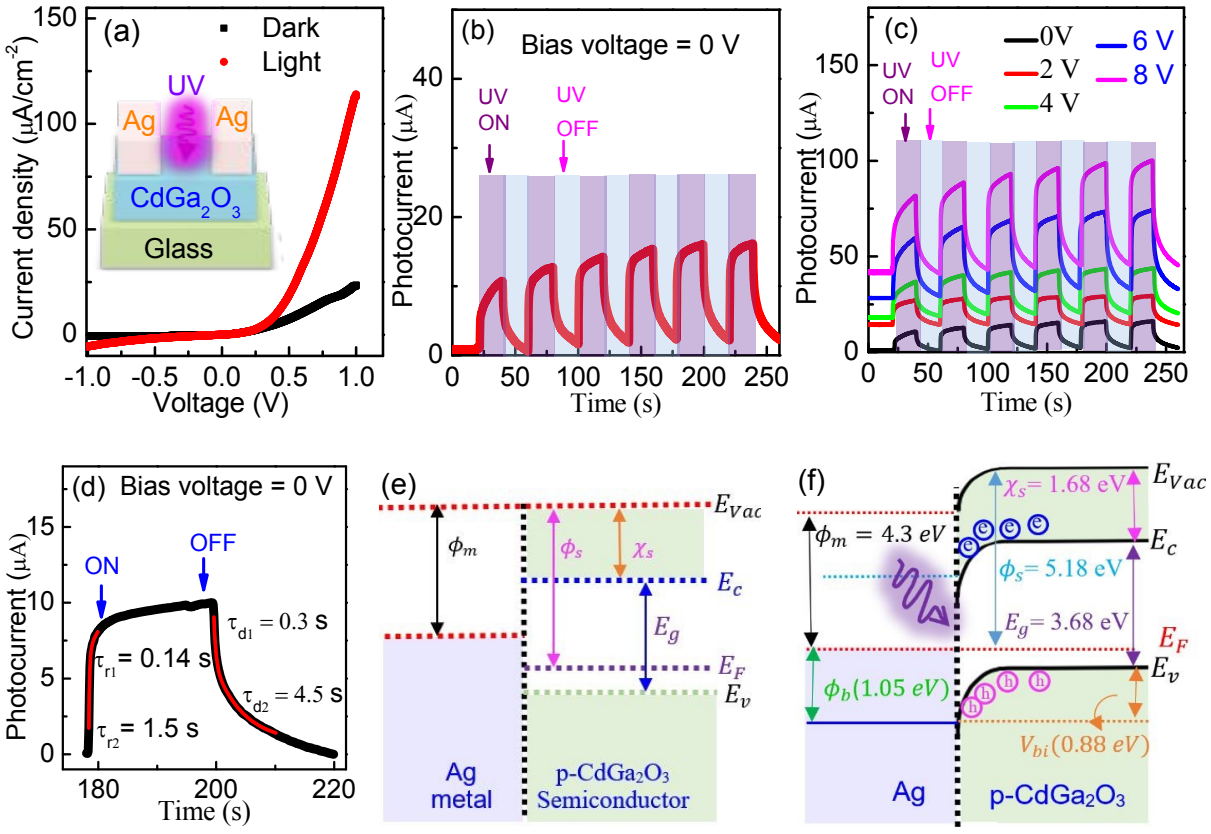

View Article Online
DOI: 10.1039/D5TC02386F

Figure 4. (a) Current-voltage characteristics of Ag/$CdGa_2O_3$ Schottky diodes. The inset of (a) shows the schematic diagram of the Ag/$CdGa_2O_3$ photodetector. (b) Photocurrent response of a typical prototype Ag/$CdGa_2O_3$ photodetector as a function of time under 365 nm light and zero bias voltage. (c) Time-dependent photocurrent response of the Ag/$CdGa_2O_3$/Ag photodetector under different bias voltage with 365 nm LED light illumination. (d) The photo response decay curve of Ag/$CdGa_2O_3$ detector are good fitted with a biexponential relaxation equation. The value of $\tau_{r1}(\tau_{d1})$ and τ_{r2} (τ_{d2}) are found to be 0.14 s (1.5s) and 0.3 s (4.5s), respectively. Energy band diagram between Ag and p-$CdGa_2O_3$ semiconductor; (e) before contact and (f) in equilibrium.

The effect of bias voltages on the photocurrent response of the Ag/$CdGa_2O_3$ photodetector was also investigated. Figure 4 (c) shows the photocurrent of Ag/$CdGa_2O_3$ Schottky photodiodes at different bias voltages. Both the I_{photo} and I_{dark} increases consistently with increases of applied voltage. The increase of dark current with the applied voltage is attributed to the increase of the drift velocity and liberation of excess carriers from the oxygen vacancy.[33] The increase in photocurrent with the applied bias voltage is due to the increase in the number of photogenerated electron-hole pairs in the film. The dynamic response of the Ag/$CdGa_2O_3$ Schottky detector exhibits excellent reproducibility and stability. The photo response decay curve of Ag/$CdGa_2O_3$ detector are good fitted with a biexponential relaxation equation, $I(t) = I_o + Aexp\left(-\frac{t}{\tau_1}\right) + Bexp\left(-\frac{t}{\tau_2}\right)$, where $I(t)$ and I_o are the current at time t and steady state photocurrent. $\tau_{r1}(\tau_{d1})$ and τ_{r2} (τ_{d2}) are the first and slow components of the rise and decay time constants, respectively, whereas A and B are fitting constants. Figure 4 (d) shows the experimental decay curve (black) along with the fitted curve (red lines). The value of $\tau_{r1}(\tau_{d1})$ and τ_{r2} (τ_{d2}) are found to be 0.14 s (1.5s) and 0.3 s (4.5s), respectively. The slow response of the photodetector is due to the existence of vacancies and structural defects formed during the growth of the $CdGa_2O_3$ film. The response time of the detector is slightly slower than the state-

View Article Online
DOI: 10.1039/D5TC02386F

of-the-art β-Ga_2O_3 photodetectors.[34, 35] we have also observed a slow decay time constant in the TRPL measurement. The slower decay lifetimes for BL and GL bands reveal that these luminescence bands are attributed to the recombination of Cd_{Ga} and V_{Ga} defect levels formed above the valence band. The response can be made fast by introducing the metal nanoparticles on the film, known as local surface plasmon resonance (LSPR), an effective method to enhance the optical absorbance and carrier excitation.[35] It has been reported that the response speed β-Ga_2O_3 photodetector has significantly increased after LSPR enhancement by Pt nanoparticles.[35] This increase in device response speed is due to the less traps in the localized interface of Pt and Ga_2O_3 and the enhancement of faster band-to-band transitions. The slow response has previously been observed in NiO/Ga_2O_3 and Ag (graphene)/β-Ga_2O_3 photodetectors, attributed to gallium vacancies and oxygen vacancies.[36, 37]

Figure 4 (e) shows the energy band diagram of Ag/$CdGa_2O_3$ Schottky photodetectors when the metal (Ag) and semiconductor ($CdGa_2O_3$) are in contact. In this band diagram, the work function of Ag and $CdGa_2O_3$ are indicated by ϕ_m and ϕ_s. The value of the work function for Ag is 4.3 eV. [38] The band edge position for $CdGa_2O_3$ with respect to vacuum level (E_{vac}) can be determined by the valence band position (E_v) following expression, $E_{vac} = V_{FB} + \phi_m + \Delta E_{FV}$, where V_{FB} is the flat band potential determined from the intercept on the voltage axis of the Mott-Schottky plot (Figure 3d) and is found to be 0.88 eV. The $\Delta E_{FV} = E_F - E_v$ is the difference between the E_v and the Fermi level (E_F). The value of ΔE_{FV} can be determined from the following relation; $\Delta E_{FV} = (kT/q)\, ln(N_V/N_A)$, where N_V, k, and T are effective hole density of states in the valence band, Boltzmann constant, and temperature, respectively. The N_A ($3.65 \times 10^{17}\ cm^{-3}$) is the acceptor concentration determined from the Mott-Schottky measurement. The value of N_V can be determined using the expression $N_V = 2\left(2\pi m_h^* kT/h^2\right)^{3/2}$, where m_h^* stand for the effective mass of hole, which was calculated from $m_h^* = 5.56\, m_o$, where m_o is the rest mas of electron.[39] The values of N_V and ΔE_{FV} for

$CdGa_2O_3$ semiconductor are 3.32×10^{20} cm^{-3} and 0.17 eV, respectively. The work function for $CdGa_2O_3$ semiconductor is determined using the expression $\phi_s = V_{FB} + \phi_m$ and is found to be 5.18 eV. The electron affinity (χ_s) is related to the work function and band gap of a semiconductor as $\phi_s = E_g + \chi_s - V_{FB}$, and the value calculated value for $CdGa_2O_3$ is found to be 1.68 eV. Figure 4(f) shows the Energy band diagram between Ag and p-$CdGa_2O_3$ semiconductor in equilibrium under illumination. As the value of ϕ_s is greater than ϕ_m, when the Ag is deposited on the $CdGa_2O_3$ thin film, electrons will move from the Ag to the $CdGa_2O_3$ film, resulting in the alignment of the Fermi levels of this metal and semiconductor, and the thermal equilibrium is obtained. As a result, the downward band bending at the interface of the $CdGa_2O_3$ is observed owing to the accumulation of uncompensated ionised acceptors near the interface, resulting in space charge formation. The built-in potential of this Schottky diode photodetector is governed by the Schottky junction formed at the interface of the Ag/$CdGa_2O_3$. This potential is responsible for the low dark current of this detector. Under the illumination of a 365 nm UV light source, the $CdGa_2O_3$ film absorbs light energy and generates a lot of electron-hole pairs. Moreover, the total built-in potential increases the separation efficiency of these electron-hole pairs, resulting in the enhancement of photocurrent and responsivity of the detector at 0 volts. Table 1 compiles the key performance parameters of the Ag/$CdGa_2O_3$ Schottky photodiode UV detector at zero bias voltage in this work, and the earlier reported self-driven photodetector is presented. The Ag/$CdGa_2O_3$ Schottky photodetector exhibits enhanced detectivity and responsivity compared to the previously reported UV self-powered photodetector.

View Article Online
DOI: 10.1039/D5TC02386F

Table 1: Summary of the key performance parameters of the $CdGa_2O_3$ film-based Schottky photodiodes with earlier reported self-powered UV photodetector.

Photodetector	Bias (volts)	τ_r (ms)	τ_d (ms)	Responsivity, R (mA/W)	Detectivity, D (Jones)	Reference
Ga_2O_3/GaN	0	7	9	72	3.32×10^{12}	[40]
Ag/Ga_2O_3	0	20	25	14.8	5.1×10^{12}	[41]
FTO/Ga_2O_3	0	2	8	9.2	5.27×10^{11}	[42]
β-Ga_2O_3/Ga:ZnO	0	210	272	0.76	…	[43]
β-Ga_2O_3/NSTO	0	210	70	2.6	…	[44]
Ag / β-Ga_2O_3	0	540	3320	0.26	2.8×10^9	[37]
β-Ga_2O_3/ZnO	0	523	32	4.12	$2.2\ 10^{12}$	[45]
NiO/Ga_2O_3	0	340	3650	0.057	5.45×10^9	[36]
Ag/a-Ga2O3	0	70	90	11.23	…	[46]
NiO/Ga_2O_3	0	240	340	0.047	3.84×10^9	[47]
NiO_x/Ga_2O_3	0	1690	320	0.40	3.0×10^{10}	[48]
p-CuSCN/n-Ga_2O_3	0	3800	260	5.5	3.8×10^{11}	[49]
Ag/$CdGa_2O_3$	0	140	300	164	7.5×10^{11}	This work

3.5 Mechanism of Hole Self-trapping Reduction and p-type Conduction

The XPS spectroscopy and total density of the state (TDOS) calculations have been studied to describe the electronic structure of the near valence band and the p-type conduction mechanism in $CdGa_2O_3$ films. Figure 5 (a) displays the valence band of X-ray photoelectron spectra for pristine and $CdGa_2O_3$ films. The spectra show that the top edge of the valence band of the $CdGa_2O_3$ film moves down to the lower energy side compared to the pristine film. This result demonstrates that Cd-induced acceptor-type defect states are generated on top of the valence band. The spectra also manifest that a tail state extended toward the Fermi level appears [displayed by dotted circle in Figure 5 (a)]. This tail state lies in the binding energy range of ~0-1.2 eV on top of the valence band. The linear extrapolation method is applied to the lower straight-line region of O 2p to determine the valence band maxima of pristine and $CdGa_2O_3$ films. The value of valence band maxima for pristine and $CdGa_2O_3$ films is 2.4 and 1.6 eV,

View Article Online
DOI: 10.1039/D5TC02386F

respectively. This result indicates a 0.8 eV upward shift of the valence band edge is observed for $CdGa_2O_3$ films compared to the pristine β-Ga_2O_3 film. Chikoidze et al. proposed that the lower energy side of the O 2p core level for p-type β-Ga_2O_3 is flat and lies within the 0-2.0 eV binding energy range. This consent agrees with the energy position of the valence band edge of 1.6 eV for $CdGa_2O_3$ as a p-type conductive material.[12]

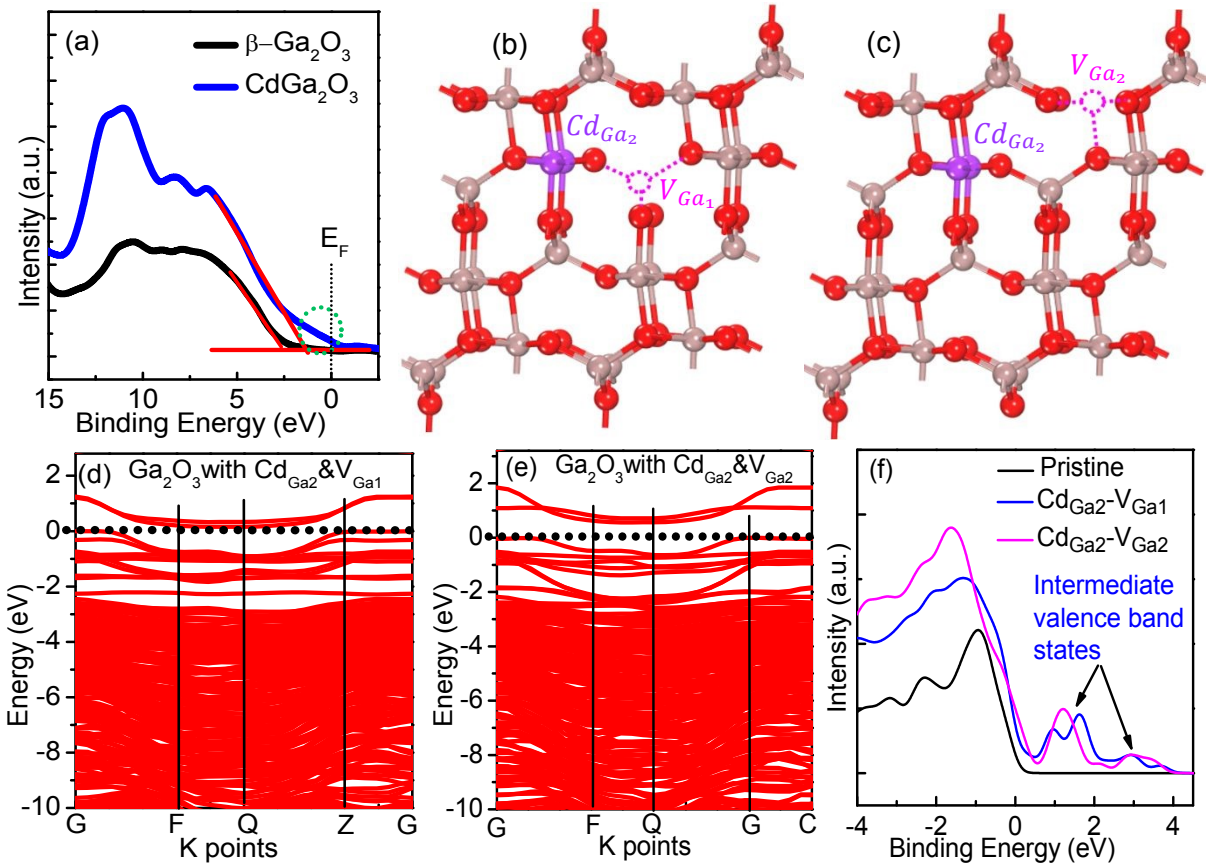

Figure 5. (a) Determination of the energy position of the valence band maximum using the linear extrapolation method. Extrapolating the linear portion of the low-energy side of O 2p core level spectra provides the valence band maximum of 2.4 and 1.6 eV for pristine and $CdGa_2O_3$ films. The atomic arrangement of a 1 x 1 x 2 β-Ga_2O_3 supercell contains (b) Cd_{Ga_2} and V_{Ga_1} , and (c) Cd_{Ga_2} and V_{Ga_2} defects. The gray and red balls are gallium and oxygen atoms, respectively. The subscript 1 and 2 indicates the tetrahedral and octahedral sites of Ga atoms, respectively. The near valence band structure of pristine β-Ga_2O_3 with (d) Cd_{Ga_2} and

View Article Online
DOI: 10.1039/D5TC02386F

V_{Ga_1}, and (e) Cd_{Ga_2} and V_{Ga_2} defects. (f) The total density of state for pristine β-Ga_2O_3 with (i) Cd_{Ga_2} and V_{Ga_1}, and (ii) Cd_{Ga_2} and V_{Ga_2}. The TDOS calculations indicate that an upward shift of the valence band edge and an intra-valence band state is observed with the formation of Cd_{Ga2} and V_{Ga2} defects in β-Ga_2O_3.

The hole self-trapping in β-Ga_2O_3 can be reduced by: (i) acceptor dopants, which have a higher atomic radius than Ga,[50] (ii) controlling the optical bandgap of this material by specific impurity doping,[51] and (iii) alloying with a material which less tendency of hole self-trapping.[50] As the atomic size of the Cd^{2+} (0.097nm) is larger compared to Ga^{3+} (0.062nm), when Cd occupies the Ga site, the lattice volume of $CdGa_2O_3$ becomes larger than the pristine β-Ga_2O_3, resulting in the reduction of hole self-trapping. As $CdGa_2O_3$ film shows V_{Ga}-related BL and Cd_{Ga}-associated GL emission bands, the Cd_{Ga} and V_{Ga} defects are intentionally incorporated in the 1x1x2 supercell of β-Ga_2O_3 to understand the near valence band electronic structure of β-Ga_2O_3 film [Figure 5 (b) and (c)]. The tetrahedral and octahedral Ga atoms are indicated by Ga_1 and Ga_2, respectively. For the incorporation of $Cd_{Ga_1(Ga_2)}$ and $V_{Ga_1(Ga_2)}$ defects, two Ga atoms are replaced by Cd atoms (2/16 = ~12 atom% Cd), and one $Ga_1(Ga_2)$ atom is removed from the supercell simultaneously. The near valence band structure of pristine β-Ga_2O_3 with (d) Cd_{Ga_2} and V_{Ga_1}, and (e) Cd_{Ga_2} and V_{Ga_2} defects has been investigated, as displayed in Figure 5 (b) and (c). The near valence band structures of β-Ga_2O_3 with (a) Cd_{Ga_1}, (b) Cd_{Ga_1} and V_{Ga_1}, (c) $Cd_{Ga_1}$and V_{Ga_2}, defects have also been studied [Figure S6 (a-c)]. The corresponding total density of state (TDOS) is shown in [Figure S6 (d)]. DFT calculations reveal that the optical band gap of pristine β-Ga_2O_3 is 4.9 eV [Figure S7 (b)]. The band gap slightly increases for the substitution of tetrahedral Ga_1 atoms with Cd (Cd_{Ga_1}) [Figure S7 (c)] and decreases when Cd occupies the octahedral Ga_2 sites (Cd_{Ga_2}) in β-Ga_2O_3 [Figure S7 (d)]. The calculations show that there are no intermediate valence band states above the Fermi level

is observed for the simultaneous formation of Cd_{Ga_1} & V_{Ga_1} defects [Figure S7 (b)] and Cd_{Ga_1} and V_{Ga_2} defects [Figure S4 (c)]. However, the simultaneous formation of Cd_{Ga_2} and V_{Ga_1} (or V_{Ga_2}) defects in β-Ga_2O_3 exhibits a significant shift of the near valence band edge [Figure 5 (d-e)], resulting the formation of an intermediate valence band state above the Fermi level [Figure 5 (f)]. These theoretical results are consistent with the near valence band of XPS spectra. Theoretical calculation and experimental observations reveal that the octahedral Ga_2 site is more favourable for Cd, and this element is preferably occupied at the Ga_2 site than the tetrahedral Ga_1 site, producing Cd_{Ga_2}, which is responsible for the green emission band in the photoluminescence spectra. The calculations also indicate that the intermediate valence band state only appears with the simultaneous formation of Cd_{Ga_2} defect and V_{Ga_1} (or V_{Ga_2}) vacancies. Therefore, the blue emission can appear due to the formation of a tetrahedral V_{Ga_1} vacancy or an octahedral V_{Ga_2} defect. Li et al. reported that the V_{Ga2} has lower formation energy than $V_{Ga1,}$ and both of them have lower formation energy than the other intrinsic defect of Ga_2O_3 at above 1 eV Fermi energy level.[52] The TDOS curves for a 1x1x2 supercell of β-Ga2O3 containing (i) Cd_{Ga_2}, (ii) Cd_{Ga_2} and V_{Ga_1}, and (iii) Cd_{Ga_2} and V_{Ga_2} are displayed in Figure 5(f). The formation of the occupied intra-valence band state leads to the downward shift of the Fermi level. The FWHM of this intra-valence state is ~1 eV and lies above the Fermi level. For pristine β-Ga_2O_3, the valence band maximum mainly arises from the O 2p states. The partial density of state for Ga, O, and Cd is shown in Figure S8. For the $CdGa_2O_3$, the occupied intra-valence band appears from the orbital contribution of Ga 2p, O 2p, and Cd 4d orbitals. We observed that the valence band edge in the β-Ga_2O_3 containing Cd_{Ga_2} and V_{Ga_2} defects is notably higher than that of the pristine β-Ga_2O_3, resulting in a decrease of the band gap and promoting *p*-type conductivity. These results are consistent with the decreasing trend of experimentally observed bandgap and p-type conduction in $CdGa_2O_3$ films. This result is consistent with the result observed by Zhang et al., they reported the Cd dopant induce a

View Article Online
DOI: 10.1039/D5TC02386F

shallow acceptor level, which contributed to the conductivity in the Cd-doped Ga_2O_3 system. The Mott-Schottky measurement confirms a significant concentration of holes in $CdGa_2O_3$ films attributed to the presence of Cd_{Ga_2} and V_{Ga_2} acceptor defects. The Franck-Condon analysis of PL spectral line shape confirms that the energy levels of Cd_{Ga_2} and V_{Ga_2} acceptor defects are 720 and 180meV, respectively, which are significantly lower than that of the energy level of 900 meV for the STHs in $CdGa_2O_3$ films. The formation of Cd_{Ga_2} and V_{Ga_2} acceptors in $CdGa_2O_3$ films reduces the STHs by competing with the formation of STH sites. The formation of these Cd_{Ga_2} and V_{Ga_2} acceptor defects in $CdGa_2O_3$ film destabilizes STHs by lowering the Fermi level, rendering it energetically less favorable for holes to be captured in STH configurations. As the values of energy levels for these acceptors are lower than that of the energy level of STHs, the holes are captured by these Cd_{Ga_2} and V_{Ga_2} acceptor levels before they can form STHs.

4. Conclusions

Ga_2O_3 and $CdGa_2O_3$ thin films were prepared by a standard atomizing spray pyrolysis technique. Both pristine and $CdGa_2O_3$ films show a monoclinic crystal structure. The Cd incorporation in β-Ga_2O_3 significantly quenches the characteristic ultraviolet luminescence, indicating the destabilization of STHs and introducing a distinct recombination channel of green luminescence attributed to Cd_{Ga} defects along with gallium vacancy (V_{Ga})-associated blue emission. The slow decay time constants of 38.45 and 13.31μs for the blue and green emission indicate that the recombination involves a conduction band electron and V_{Ga} and Cd_{Ga} defects for these emissions. First-principle calculations reveal that incorporating Cd in β-Ga_2O_3 forms Cd_{Ga} and V_{Ga} defects, which leads to an intravalence band state adequately high in energy to promote p-type conductivity in $CdGa_2O_3$ film. These acceptor defects lower the Fermi level and make it energetically unfavourable for holes to be trapped in the STHs configuration. The

Mott-Schottky measurement also supports the p-type conductivity in this film. This p-type $CdGa_2O_3$ film is inserted into a Schottky diode to fabricate an $Ag/CdGa_2O_3$ photodetector, which operates as an efficient UV photodetector with a responsivity of 164 mA/W and a detectivity of 7.75×10^{11} Jones. The results suggest that the p-type $CdGa_2O_3$ film can be exploited in optoelectronic applications that require ultraviolet detection without an external power supply.

Data Availability Statement

The data that support the findings of this study are available from the corresponding author upon reasonable request.

Author Contributions

Tasfia Chowdhury: Writing – original draft (equal); Data curation (equal); Formal analysis (equal); **Rahima Khatun**: Writing – original draft (equal); Data curation (equal); Formal analysis (equal), Software (supporting), Data curation (lead). **Md. Rabiur Rahaman**: Data curation (supporting). **Md. Azizar Rahman**: Writing – review & editing (lead); Investigation (lead); Conceptualization (lead); Supervision (lead).

Conflict of Interest

The authors have no conflicts to disclose.

Acknowledgements

The authors greatly acknowledge the financial support of the Committee for Advanced Studies and Research (CASR), Bangladesh University of Engineering and Technology (BUET). The authors are also thankful to the Department of Physics, BUET, for allowing us to use different equipment for this research. This work is partially supported by a grant from UNESCO-TWAS,

View Article Online
DOI: 10.1039/D5TC02386F

the Swedish International Development and Cooperation Agency (SIDA), and the Ministry of Science and Technology, Government of Bangladesh.

References

1. M. Bosi, P. Mazzolini, L. Seravalli and R. Fornari, *J. Mater. Chem. C*, 2020, **8**, 10975-10992.
2. M.-G. Ju, X. Wang, W. Liang, Y. Zhao and C. Li, *J. Mater. Chem. A*, 2014, **2**, 17005-17014.
3. E. Chikoidze, T. Tchelidze, C. Sartel, Z. Chi, R. Kabouche, I. Madaci, C. Rubio, H. Mohamed, V. Sallet and F. Medjdoub, *Mater. Today Phys.*, 2020, **15**, 100263.
4. E. Chikoidze, C. Sartel, H. Mohamed, I. Madaci, T. Tchelidze, M. Modreanu, P. Vales-Castro, C. Rubio, C. Arnold and V. Sallet, *J. Mater. Chem. C*, 2019, **7**, 10231-10239.
5. M. D. McCluskey, *J. Appl. Phys.*, 2020, **127**,101101 .
6. J. B. Varley, A. Janotti, C. Franchini and C. G. Van de Walle, *Phys. Rev. B*, 2012, **85**, 081109.
7. C. Yan, J. Su, Y. Wang, Z. Lin, J. Zhang, J. Chang and Y. Hao, *J. Alloys Compd.*, 2021, **854**, 157247.
8. X. Wang, F. Zhang, K. Saito, T. Tanaka, M. Nishio and Q. Guo, *J. Phys. Chem. Solids*, 2014, **75**, 1201-1204.
9. S. Luan, L. Dong, X. Ma and R. Jia, *J.Alloys Compd.*, 2020, **812**, 152026.
10. C. Tang, J. Sun, N. Lin, Z. Jia, W. Mu, X. Tao and X. Zhao, *RSC Adv.*, 2016, **6**, 78322-78334.
11. T. Onuma, S. Fujioka, T. Yamaguchi, M. Higashiwaki, K. Sasaki, T. Masui and T. Honda, *Appl. Phys. Lett.*, 2013, **103**, 041910.
12. E. Chikoidze, A. Fellous, A. Perez-Tomas, G. Sauthier, T. Tchelidze, C. Ton-That, T. T. Huynh, M. Phillips, S. Russell and M. Jennings, *Mater. Today Phys.*, 2017, **3**, 118-126.
13. X. Xiao, L. Liang, Y. Pei, J. Yu, H. Duan, T.-C. Chang and H. Cao, *Appl. Phys. Lett.*, 2020, **116**, 192102 .
14. C. P. Liu, C. Y. Ho, R. Dos Reis, Y. Foo, P. F. Guo, J. A. Zapien, W. Walukiewicz and K. M. Yu, *ACS Appl. Mater. Interfaces*, 2018, **10**, 7239-7247.
15. X. Ma, B. Lu, D. Li, R. Shi, C. Pan and Y. Zhu, *J. Phys. Chem. C*, 2011, **115**, 4680-4687.
16. M. Segall, P. J. Lindan, M. a. Probert, C. J. Pickard, P. J. Hasnip, S. Clark and M. Payne, *J. Condens. Matter Phys.*, 2002, **14**, 2717.
17. K. Huang and A. Rhys, *Proc. R. Soc. Lond. A Math. Phys. Sci.* , 1950, **204**, 406-423.
18. A. Alkauskas, M. D. McCluskey and C. G. Van de Walle, *J. Appl. Phys.*, 2016, **119**, 181101.
19. X. Sun, K. Liu, X. Chen, Q. Hou, Z. Cheng, J. Yang, Q. Ai, Y. Zhu, B. Li and L. Liu, *J. Mater. Chem. C*, 2023, **11**, 3227-3234.
20. P. Zhou, Z. Le, Y. Xie, J. Fang and J. Xu, *J. Alloys Compd.*, 2017, **692**, 170-177.
21. A. Navarro-Quezada, S. Alamé, N. Esser, J. Furthmüller, F. Bechstedt, Z. Galazka, D. Skuridina and P. Vogt, *Phys. Rev. B*, 2015, **92**, 195306.
22. L. Cheng, Y. Zhu, W. Wang and W. Zheng, *J. Phys. Chem. Lett.*, 2022, **13**, 3053-3058.
23. C. P. Irvine, A. Stopic, M. T. Westerhausen, M. R. Phillips and C. Ton-That, *Phys. Rev. Mater.*, 2022, **6**, 114603.
24. M. Reshchikov, J. D. McNamara, F. Zhang, M. Monavarian, A. Usikov, H. Helava, Y. Makarov and H. Morkoç, *Phys. Rev. B*, 2016, **94**, 035201.
25. Y. Y. Tay, T. Tan, F. Boey, M. H. Liang, J. Ye, Y. Zhao, T. Norby and S. Li, *Phys. Chem. Chem. Phys.*, 2010, **12**, 2373-2379.

26. C. F. Klingshirn, A. Waag, A. Hoffmann and J. Geurts, *Zinc Oxide: From Fundamental Properties Towards Novel Applications*, Springer Berlin Heidelberg, 2010.
27. H. He, Z. Ye, S. Lin, B. Zhao, J. Huang and H. Tang, *J. Phys. Chem. C*, 2008, **112**, 14262-14265.
28. T. Chowdhury, D. K. Paul, M. R. Rahaman, C. Ton-That and M. A. Rahman, *J. Alloys Compd.*, 2025, **1010**, 177609.
29. K. Gelderman, L. Lee and S. Donne, *J. Chem. Edu.*, 2007, **84**, 685.
30. A. Fiedler, R. Schewski, Z. Galazka and K. Irmscher, *ECS J. Solid State Sci. Technol.*, 2019, **8**, Q3083.
31. W.-Y. Kong, G.-A. Wu, K.-Y. Wang, T.-F. Zhang, Y.-F. Zou, D.-D. Wang and L.-B. Luo, *Adv. Mater.*, 2016, **28**, 10725-10731.
32. S. Kim, S. Oh and J. Kim, *ACS Photonics*, 2019, **6**, 1026-1032.
33. D. Guo, Y. Su, H. Shi, P. Li, N. Zhao, J. Ye, S. Wang, A. Liu, Z. Chen and C. Li, *ACS Nano*, 2018, **12**, 12827-12835.
34. M. Zhang, J. Wu, H. Lin, X. Zhang, J.-L. Xu, Y. Yan, S.-D. Wang, M. Wong and H.-S. Kwok,*IEEE Electron Device Lett.*, 2021, **42**, 998-1001.
35. Z. Liu, S.-L. Sha, G.-H. Shen, M.-M. Jiang, M.-L. Zhang, Y.-F. Guo and W.-H. Tang, *IEEE Electron Device Lett.*, 2023, **44**, 1324-1327.
36. Y. Wang, C. Wu, D. Guo, P. Li, S. Wang, A. Liu, C. Li, F. Wu and W. Tang, *ACS Appl. Electron. Mater.*, 2020, **2**, 2032-2038.
37. C. Wu, C. He, D. Guo, F. Zhang, P. Li, S. Wang, A. Liu, F. Wu and W. Tang, *Mater. Today Phys.*, 2020, **12**, 100193.
38. A. Kumatani, Y. Li, P. Darmawan, T. Minari and K. Tsukagoshi, *Sci. Rep.*, 2013, **3**, 1026.
39. A. Mock, R. Korlacki, C. Briley, V. Darakchieva, B. Monemar, Y. Kumagai, K. Goto, M. Higashiwaki and M. Schubert, *Phys. Rev. B*, 2017, **96**, 245205.
40. W. Chen, X. Xu, M. Li, S. Kuang, K. H. Zhang and Q. Cheng, *Adv. Opt. Mater.*, 2023, **11**, 2202847.
41. P. Tan, X. Zhao, X. Hou, Y. Yu, S. Yu, X. Ma, Z. Zhang, M. Ding, G. Xu and Q. Hu, *Adv. Opt. Mater.*, 2021, **9**, 2100173.
42. Y. Li, Z. Zhou, H. Pan, J. Chen, Y. Wang, Q. Qu, D. Zhang, M. Li, Y. Lu and Y. He, *J. Mater. Res. Technol.*, 2023, **22**, 2174-2185.
43. Z. Wu, L. Jiao, X. Wang, D. Guo, W. Li, L. Li, F. Huang and W. Tang, *J. Mater. Chem. C*, 2017, **5**, 8688-8693.
44. G. Daoyou, L. Han, L. Peigang, W. Zhenping, W. Shunli, C. Can, L. Chaorong and T. Weihua, *ACS Appl. Mater. Interfaces* 2017, **9**, 1619–1628.
45. T. Mei, S. Li, S. Zhang, Y. Liu and P. Li, *Phys. Scr.*, 2022, **97**, 015808.
46. C. Yu, H. Li, K. Ding, L. Huang, H. Zhang, D. Pang, Y. Xiong, P. A. Yang, L. Fang and W. Li, *Adv. Opt. Mater.*, 2024, **12**, 2400116.
47. M. Amari, O. H. AL-Zoubi, P. Bansal, H. Kaur, A. A. Telba, E. M. Awwad, A. Kumar, M. S. Alhassan and M. K. Abosaoda, *Sens. Actuators A: Phys.*, 2024, **373**, 115360.
48. J. M. T. Vasquez, A. Ashai, Y. Lu, V. Khandelwal, M. Rajbhar, M. Kumar, X. Li and B. Sarkar, *J. Phys. D: Appl. Phys.*, 2023, **56**, 065104.
49. B. Sun, W. Sun, S. Li, G. Ma, W. Jiang, Z. Yan, X. Wang, Y. An, P. Li and Z. Liu, *Opt. Commun.*, 2022, **504**, 127483.
50. X. Cai, F. P. Sabino, A. Janotti and S.-H. Wei, *Phys. Rev. B*, 2021, **103**, 115205.
51. F. Matar, Y.-L. Shi, F. C.-C. Ling, A. Salih, C. P. Irvine, S. De Silva, M. R. Phillips and C. Ton-That, *J. Alloys Compd.*, 2023, **960**, 170983.
52. Q. Li, J. Zhao, Y. Li, X. Guan, Z. Jia, N. Lin and X. Zhao, *J. Phys. Chem. C*, 2024, **128**, 11817-11826.
53. C. Zhang, X. Fu and H. Wang, *Mater. Today Commun.*, 2025, **42**, 111524.

View Article Online
DOI: 10.1039/D5TC02386F

View Article Online
DOI: 10.1039/D5TC02386F

Data availability

The experimental and theoretical data that support the findings of this investigation are available from the corresponding author upon request.